

# Discrete Knot Theory via Lattice-Filtered Move Graphs

Makoto Ozawa

## Abstract

We introduce *lattice-filtered move graphs* as finite-state experimental models for knot types. At level  $N$ , vertices are lattice-polygon representatives of a fixed knot type with lattice length at most  $N$ , modulo orientation-preserving lattice isometries, and edges are prescribed local moves. Connected components of these graphs are discrete analogues of admissible components in ropelength-filtered knot spaces. The first level at which two initial components become connected defines a discrete merge scale; after subtracting the birth level, the resulting function is an ultrapseudometric whenever the relevant initial components eventually merge.

The theoretical part is deliberately move-system independent. We then specialize to the simple cubic lattice and to BFACF-type moves, treating BFACF as a chosen local move system rather than as a complete lattice-isotopy calculus. A separate conditional theorem shows that, for PL-realizable local move systems, discrete paths project to finite Reidemeister certificates. This PL-realizability hypothesis is stated explicitly; it is not used to justify the BFACF computations unless verified separately for the particular BFACF implementation.

The experimental part reports reproducible seed-generated computations from a prototype Python implementation. The main calculation starts with a 30-edge simple cubic lattice seed  $\omega$  for the figure-eight knot and its reflected mirror seed  $\omega!$ . With mirror symmetries not identified, the two seed-generated BFACF components are separated at the birth level  $N = 30$  and merge at  $N = 32$ . Thus, relative to the supplied seeds and the BFACF move system,

$$m_{\text{seed}}^{\text{BFACF}}(\omega, \omega!) = 32.$$

This is a seed-specific and BFACF-specific length-barrier computation, not a claim about the global merge matrix of the full minimal layer  $I_{\text{SC}}(4_1)$ . Additional checks for the trefoil, the five-crossing prime knots, and composite trefoil examples are included as reproducibility tests and as evidence for further experimental questions about local rigidity in birth-level lattice move graphs.

**Keywords.** Lattice knots, ropelength, filtered knot spaces, local move graphs, BFACF moves, cubulated moves, merge scales, finite recognition.

**2020 Mathematics Subject Classification.** 57K10; 57K12; 05C10; 68R10; 49Q10.

## 1 Introduction

The ropelength-filtered approach to knot theory studies a knot type through the geometry of its thick representatives. For a knot type  $K$  and a parameter  $\Lambda > 0$ , consider the space

$$Y_\Lambda(K) = \{\gamma \in K \mid \text{Thi}(\gamma) = 1, \text{Len}(\gamma) \leq \Lambda\} / \text{Isom}^+(\mathbb{R}^3).$$

Two representatives are called admissibly equivalent at scale  $\Lambda$  if they can be joined by a path remaining in  $Y_\Lambda(K)$ . Thus the admissible components are the path components of  $Y_\Lambda(K)$ , and as  $\Lambda$  increases these components form a persistence object. The first level at which the space is non-empty is the ropelength level  $\text{Rop}(K)$ , and the initial layer

$$I(K) = Y_{\text{Rop}(K)}(K)$$

may be regarded as the ideal stratum of  $K$ . This continuous ropelength-filtered framework, including ideal strata, admissible components, and merge scales, was developed in [12]. The present paper is intended as an experimental, computable lattice analogue of that framework. For the reader's convenience, the constructions needed below are recalled in self-contained form; no result of [12] is used as a black box except for the motivating terminology and comparison with the continuous theory.

This continuous theory is conceptually natural, but it is difficult to compute. Even deciding the number of admissible components of  $Y_\Lambda(K)$  at a fixed scale is generally out of reach. Likewise, the merge scale of two components, namely the first value of  $\Lambda$  at which they become joined in the filtered space, is not directly computable from the definition.

The aim of this paper is to introduce a discrete model in which the same ideas can be implemented by finite graph algorithms. The basic replacement is

$$\text{admissible deformation} \quad \rightsquigarrow \quad \text{finite sequence of local moves,}$$

and

$$\text{admissible component} \quad \rightsquigarrow \quad \text{connected component of a finite move graph.}$$

The resulting framework is called *discrete knot theory* in this paper.

The experimental point of view is essential here. The simplest useful objects are not only the full graphs  $G_N$ , which may be too large to enumerate, but also the subgraphs generated from specified seed representatives. These seed-generated graphs are reproducible finite approximations to local regions of the filtered state space. They allow one to ask concrete questions such as: when do two mirror-related lattice representatives first become connected after allowing temporary length expansion?

Our most informative test case is the figure-eight knot. Although  $4_1$  is amphichiral as an ordinary knot, a 30-edge simple cubic lattice seed and its reflected mirror seed lie in distinct BFACF components at the minimal length level  $N = 30$ . A bidirectional search finds a connecting state at  $N = 32$ , so the BFACF seed-generated merge scale is  $m_{\text{seed}}^{\text{BFACF}}(4_1, 4_1!) = 32$ . This experiment illustrates the basic phenomenon studied in the paper: a topological equivalence can have a positive barrier relative to a specified filtered lattice move graph. The statement is not a claim about all minimal representatives of  $4_1$ , nor about a complete lattice isotopy move system.

The main example uses lattice knots. Let  $\mathcal{L}$  be a regular cubic lattice, for instance the simple cubic lattice  $\mathbb{Z}^3$ . A lattice knot is a self-avoiding closed polygon whose edges are lattice edges. For a knot type  $K$ , let

$$\mathcal{P}_N^\mathcal{L}(K) = \{\omega \subset \mathcal{L} \mid \omega \text{ is a lattice polygon of type } K, \ell(\omega) \leq N\} / \text{Isom}(\mathcal{L}),$$

where  $\ell(\omega)$  is the number of lattice edges. If chirality is to be kept fixed, one should quotient by the orientation-preserving lattice isometry group; if mirror images are to be identified, one may quotient by the full lattice isometry group. Choose a finite set of local moves, for example BFACF-type moves or cubulated moves. We then define a finite graph

$$G_N^\mathcal{L}(K)$$

whose vertices are the elements of  $\mathcal{P}_N^\mathcal{L}(K)$  and whose edges are given by the allowed moves. The connected components

$$\pi_0(G_N^\mathcal{L}(K))$$

are the lattice admissible components at level  $N$ .

This construction should not be interpreted as a canonical discretization of ropelength. A lattice polygon has corners and does not literally satisfy  $\text{Thi} = 1$  as a smooth curve. Rather, the lattice-filtered graph is a computable combinatorial surrogate for the ropelength-filtered space.

It captures the same structural pattern: representatives are filtered by size, deformations are constrained by the same size bound, and components merge when the size bound is increased.

There is a second, equally important qualification. The connected components are components for the chosen move system. In the computations below this move system is BFACF. We use BFACF moves because they are standard in lattice-polygon sampling and because they give a reproducible finite graph, but no BFACF completeness theorem is assumed. A larger or complete move system could identify components earlier.

The paper also clarifies the relation between the present discrete theory and a finite recognition theory based on diagrams and Reidemeister moves. The three levels are as follows:

continuous ropelength theory	:	geometry of $Y_\Lambda(K)$ ,
finite knot theory	:	finite diagrammatic recognition data,
discrete knot theory	:	finite state spaces and local move graphs.

Finite knot theory is a theory of finite certificates; discrete knot theory is a theory of computable finite state models. They are related but not identical.

**Organization.** Sections 2–4 give the abstract filtered-graph formalism and its lattice specialization. Section 5 compares the continuous, finite-certificate, and discrete-state-space viewpoints. Section 6 records the conditional PL-realizability statement needed to turn realized discrete paths into finite Reidemeister certificates. Section 8 explains the coarse relation with ropelength-filtered spaces and states the convergence problem. Sections 9 and 10 describe the prototype implementation and the reproducible seed-generated experiments. Section 11 records problems and experimental conjectures suggested by the computations.

## Main contributions

The contributions of this paper are the following.

- (1) We define abstract filtered local-move models for knot types and their level- $N$  move graphs.
- (2) We define discrete admissible components, seed-generated reachable graphs, and discrete merge scales.
- (3) We prove that finite merge scales on the initial layer give an ultrapseudometric after subtracting the birth level.
- (4) We construct the simple cubic lattice model using BFACF-type moves, while making explicit that all BFACF components and merge scales are relative to this chosen move system.
- (5) Under an explicit PL-realizability hypothesis on the local moves, we explain how move paths give finite diagrammatic certificates.
- (6) We report reproducible seed-generated computations for  $3_1$ ,  $4_1$ ,  $4_1!$ ,  $5_1$ ,  $5_2$ , and composite trefoil examples.
- (7) We verify the BFACF seed-generated merge scale  $m_{\text{seed}}^{\text{BFACF}}(4_1, 4_1!) = 32$  for a specified figure-eight seed and its reflected mirror seed.
- (8) We state experimental problems and conjectures suggested by the data, including positive BFACF length barriers for amphichiral knots in specified lattice-filtered move graphs.

## 2 Abstract filtered local-move models

We begin with an abstract formulation. This keeps the main results independent of the choice of lattice or move system.

**Definition 2.1** (Filtered local-move model). Let  $K$  be a knot type. A *filtered local-move model* for  $K$  is a triple

$$\mathfrak{D}(K) = (\mathcal{S}(K), \mathcal{M}, \ell),$$

where:

- (i)  $\mathcal{S}(K)$  is a countable set of finite representatives of  $K$ ;
- (ii)  $\mathcal{M}$  is a symmetric set of local moves between elements of  $\mathcal{S}(K)$ , each move preserving the knot type  $K$ ;
- (iii)  $\ell : \mathcal{S}(K) \rightarrow \mathbb{N}$  is a complexity function;
- (iv) for every  $N$ , the set

$$\mathcal{S}_N(K) = \{x \in \mathcal{S}(K) \mid \ell(x) \leq N\}$$

is finite.

The associated graph is defined as follows.

**Definition 2.2** (Filtered move graph). For a filtered local-move model  $\mathfrak{D}(K)$ , define the level- $N$  graph

$$G_N^{\mathfrak{D}}(K)$$

by

$$V(G_N^{\mathfrak{D}}(K)) = \mathcal{S}_N(K),$$

with an edge between  $x$  and  $y$  if and only if  $x$  and  $y$  differ by one allowed move in  $\mathcal{M}$ .

**Definition 2.3** (Seed-generated component and explored subgraph). Let  $x \in \mathcal{S}_N(K)$ . The *seed-generated component* at level  $N$ , denoted

$$C_N^{\text{seed}}(x) \subset G_N^{\mathfrak{D}}(K),$$

is the connected component of  $x$  in  $G_N^{\mathfrak{D}}(K)$ . In an actual computation one may stop after a vertex or time cap. The resulting explored subgraph will be denoted by

$$E_N^{\text{seed}}(x) \subset C_N^{\text{seed}}(x).$$

Thus an exhaustive computation gives  $E_N^{\text{seed}}(x) = C_N^{\text{seed}}(x)$ , whereas a capped computation records only a certified finite part of the component.

**Definition 2.4** (Seed-generated merge scale). Let  $x, y \in I_{\mathfrak{D}}(K)$  be two chosen initial representatives. The *seed-generated merge scale*  $m_{\text{seed}}(x, y)$  is the first level  $N$  such that  $x$  and  $y$  lie in the same component of  $G_N^{\mathfrak{D}}(K)$ . A positive search certificate gives an upper bound, and an exhaustive separation certificate at a level gives a lower bound. If a capped search finds no path, the outcome is recorded as inconclusive.

Seed-generated data are weaker than complete computations of  $G_N^{\mathfrak{D}}(K)$ , but they are often the computationally accessible objects. Throughout the experimental sections below, all capped searches are identified explicitly.

Since  $\mathcal{S}_N(K) \subset \mathcal{S}_{N+1}(K)$ , the graphs form a nested sequence of induced subgraphs:

$$G_N^{\mathfrak{D}}(K) \subset G_{N+1}^{\mathfrak{D}}(K) \subset G_{N+2}^{\mathfrak{D}}(K) \subset \cdots$$

**Definition 2.5** (Discrete admissible components). The *discrete admissible components* of  $K$  at level  $N$  in the model  $\mathfrak{D}$  are the connected components of  $G_N^{\mathfrak{D}}(K)$ :

$$\pi_0^{\mathfrak{D}}(K; N) = \pi_0(G_N^{\mathfrak{D}}(K)).$$

**Proposition 2.6** (Component persistence). *The inclusions*

$$G_N^{\mathfrak{D}}(K) \subset G_{N+1}^{\mathfrak{D}}(K)$$

*induce maps*

$$\pi_0(G_N^{\mathfrak{D}}(K)) \longrightarrow \pi_0(G_{N+1}^{\mathfrak{D}}(K)).$$

*Thus the discrete admissible components form a one-parameter persistence object.*

*Proof.* Every connected component of  $G_N^{\mathfrak{D}}(K)$  is contained in a connected component of  $G_{N+1}^{\mathfrak{D}}(K)$ , because the former graph is a subgraph of the latter. This gives the asserted map on connected components. Functoriality for successive inclusions is immediate.  $\square$

### 3 Initial layers and merge scales

The analogue of the ropelength birth level is the minimal complexity level.

**Definition 3.1** (Initial level and discrete ideal layer). Let

$$N_0^{\mathfrak{D}}(K) = \min\{N \in \mathbb{N} \mid \mathcal{S}_N(K) \neq \emptyset\}.$$

The *discrete ideal layer* is

$$I_{\mathfrak{D}}(K) = \mathcal{S}_{N_0^{\mathfrak{D}}(K)}(K).$$

The corresponding initial component set is

$$\mathcal{C}_0^{\mathfrak{D}}(K) = \pi_0(G_{N_0^{\mathfrak{D}}(K)}^{\mathfrak{D}}(K)).$$

**Definition 3.2** (Discrete merge scale). Let  $C, D \in \mathcal{C}_0^{\mathfrak{D}}(K)$ . The *discrete merge scale* of  $C$  and  $D$  is

$$m_{\mathfrak{D}}(C, D) = \min\{N \geq N_0^{\mathfrak{D}}(K) \mid C \text{ and } D \text{ have the same image in } \pi_0(G_N^{\mathfrak{D}}(K))\},$$

if such an  $N$  exists, and  $m_{\mathfrak{D}}(C, D) = \infty$  otherwise.

In most natural knot-complete models, every pair of initial components eventually merges. However, allowing the value  $\infty$  keeps the definition valid without assuming global completeness of the move system.

**Theorem 3.3** (Merge ultrapseudometric). *Assume that  $m_{\mathfrak{D}}(C, D) < \infty$  for all  $C, D \in \mathcal{C}_0^{\mathfrak{D}}(K)$ . Then*

$$d_{\mathfrak{D}}(C, D) = m_{\mathfrak{D}}(C, D) - N_0^{\mathfrak{D}}(K)$$

*defines an ultrapseudometric on  $\mathcal{C}_0^{\mathfrak{D}}(K)$ ; that is,*

$$d_{\mathfrak{D}}(C, C) = 0,$$

$$d_{\mathfrak{D}}(C, D) = d_{\mathfrak{D}}(D, C),$$

*and*

$$d_{\mathfrak{D}}(C, E) \leq \max\{d_{\mathfrak{D}}(C, D), d_{\mathfrak{D}}(D, E)\}.$$

*Proof.* Reflexivity and symmetry are immediate from the definition. For the strong triangle inequality, let

$$A = m_{\mathfrak{D}}(C, D), \quad B = m_{\mathfrak{D}}(D, E),$$

and put  $M = \max\{A, B\}$ . At level  $M$ , the images of  $C$  and  $D$  lie in the same component, and the images of  $D$  and  $E$  lie in the same component. Hence the images of  $C$  and  $E$  lie in the same component of  $G_M^{\mathfrak{D}}(K)$ . Therefore

$$m_{\mathfrak{D}}(C, E) \leq M.$$

Subtracting  $N_0^{\mathfrak{D}}(K)$  gives the desired inequality.  $\square$

**Remark 3.4.** The proof uses only the nested nature of the filtered graphs. Thus the ultraseudometric is not special to lattice knots; it is a general consequence of component persistence.

## 4 The lattice-filtered model

We now specialize the abstract framework to lattice knots.

### 4.1 Lattice polygons

Let  $\mathcal{L}$  be a three-dimensional lattice, such as the simple cubic lattice  $\mathbb{Z}^3$ , the face-centered cubic lattice, or the body-centered cubic lattice. A *lattice polygon* is a simple closed polygonal curve whose edges are lattice edges. Its *lattice length*  $\ell(\omega)$  is the number of lattice edges in  $\omega$ .

For a knot type  $K$ , let

$$\mathcal{P}^{\mathcal{L}}(K) = \{\omega \subset \mathcal{L} \mid \omega \text{ is a lattice polygon of knot type } K\} / \text{Isom}(\mathcal{L}),$$

where  $\text{Isom}(\mathcal{L})$  denotes the group of lattice isometries. For  $N \in \mathbb{N}$ , put

$$\mathcal{P}_N^{\mathcal{L}}(K) = \{\omega \in \mathcal{P}^{\mathcal{L}}(K) \mid \ell(\omega) \leq N\}.$$

**Lemma 4.1** (Finiteness). *For each  $N$ , the set  $\mathcal{P}_N^{\mathcal{L}}(K)$  is finite.*

*Proof.* A lattice polygon of length at most  $N$  has at most  $N$  edges. After quotienting by translations, one may place one vertex at the origin. There are only finitely many edge-direction sequences of length at most  $N$  in a fixed lattice, and only finitely many of these close up and give self-avoiding polygons. Quotienting further by the finite point group of the lattice preserves finiteness.  $\square$

### 4.2 Local move systems

There are several natural choices of local moves.

**Example 4.2** (BFACF-type moves). In the simple cubic lattice, BFACF moves are local modifications of lattice polygons that preserve the knot type when the resulting polygon remains self-avoiding. They include length-preserving moves and length-changing moves. They are widely used in Monte Carlo sampling of lattice polygons and minimal lattice knots.

**Remark 4.3** (Completeness is not assumed). The preceding statement is local: each valid BFACF move preserves the knot type. It is not a deterministic completeness theorem saying that any two lattice polygons of the same knot type are connected by BFACF moves. The present paper therefore treats BFACF as a chosen move system, and all BFACF components and BFACF merge scales are relative to that choice. If a larger move system  $\mathcal{M}' \supset \text{BFACF}$  is used, components may merge no later than they do in the BFACF graph. Thus a BFACF merge

scale is, in general, an upper bound for the corresponding merge scale in a larger complete move system, whenever such a comparison is defined.

Completeness and PL-realizability are separate issues. The experiments below use BFACF as a graph-generating rule. They do not require a proof that every BFACF move in the implementation is realized by a uniformly controlled ambient PL isotopy, and no such verification is claimed here. Section 6 explains what additional hypothesis would be needed to interpret an arbitrary move path as a finite Reidemeister certificate.

**Example 4.4** (Cubulated moves). For cubic knots, cubulated moves form a discrete analogue of Reidemeister moves. In this setting, isotopy of cubic knots can be characterized by the existence of a finite sequence of cubulated moves [6]. This example is included to emphasize that completeness is a property of a chosen move system and must be cited or proved separately from knot-type preservation of individual moves.

**Definition 4.5** (Lattice-filtered move graph). Fix a lattice  $\mathcal{L}$  and a local move system  $\mathcal{M}_{\mathcal{L}}$ . The *lattice-filtered move graph* of  $K$  at level  $N$  is the graph

$$G_N^{\mathcal{L}, \mathcal{M}}(K)$$

with vertex set  $\mathcal{P}_N^{\mathcal{L}}(K)$  and with an edge between two vertices if they differ by one move in  $\mathcal{M}_{\mathcal{L}}$ .

By the finiteness lemma,  $G_N^{\mathcal{L}, \mathcal{M}}(K)$  is a finite graph. Thus its connected components and merge scales are computable by finite graph algorithms, at least in principle.

**Definition 4.6** (Lattice admissible components). The *lattice admissible components* of  $K$  at lattice length  $N$  are

$$\pi_0^{\mathcal{L}, \mathcal{M}}(K; N) = \pi_0(G_N^{\mathcal{L}, \mathcal{M}}(K)).$$

**Definition 4.7** (Minimal lattice layer). Let

$$n_{\mathcal{L}}(K) = \min\{N \mid \mathcal{P}_N^{\mathcal{L}}(K) \neq \emptyset\}.$$

The *minimal lattice layer* is

$$I_{\mathcal{L}}(K) = \mathcal{P}_{n_{\mathcal{L}}(K)}^{\mathcal{L}}(K).$$

This is the lattice analogue of the ropelength ideal stratum.

**Definition 4.8** (Lattice merge scale). For two components

$$C, D \in \pi_0(G_{n_{\mathcal{L}}(K)}^{\mathcal{L}, \mathcal{M}}(K)),$$

define

$$m_{\mathcal{L}, \mathcal{M}}(C, D) = \min\{N \geq n_{\mathcal{L}}(K) \mid C, D \text{ have the same image in } \pi_0(G_N^{\mathcal{L}, \mathcal{M}}(K))\},$$

if such an  $N$  exists.

**Corollary 4.9** (Lattice merge ultrapseudometric). *If every pair of initial lattice components eventually merges, then*

$$d_{\mathcal{L}, \mathcal{M}}(C, D) = m_{\mathcal{L}, \mathcal{M}}(C, D) - n_{\mathcal{L}}(K)$$

*defines an ultrapseudometric on the set of components of the minimal lattice layer.*

*Proof.* This is a direct application of Theorem 3.3 to the filtered local-move model  $\mathfrak{D} = (\mathcal{P}^{\mathcal{L}}(K), \mathcal{M}_{\mathcal{L}}, \ell)$ .  $\square$

## 5 Continuous, finite, and discrete knot theories

We now clarify the relation among the three theories.

## 5.1 Continuous ropelength theory

The continuous theory studies the spaces

$$Y_\Lambda(K) = \{\gamma \in K \mid \text{Thi}(\gamma) = 1, \text{Len}(\gamma) \leq \Lambda\} / \text{Isom}^+(\mathbb{R}^3).$$

This is the continuous model introduced in [12] that motivates the lattice-filtered construction studied here. Its basic objects are:

- (i) the ideal stratum  $I(K) = Y_{\text{Rop}(K)}(K)$ ;
- (ii) admissible components  $\pi_0(Y_\Lambda(K))$ ;
- (iii) merge scales between components;
- (iv) persistence of components as  $\Lambda$  increases.

This is the geometric source of the theory.

## 5.2 Finite knot theory

In this paper, the term *finite knot theory* is used as a descriptive label for finite recognition data extracted from continuous or discrete representatives; it is not meant to denote a previously established independent subfield. A typical construction fixes a generic direction  $u \in S^2$  and sends a representative  $\gamma$  to its diagram  $D_u(\gamma)$ . For a generic one-parameter admissible deformation, the diagram changes by a finite sequence of Reidemeister moves. Thus a path in  $Y_\Lambda(K)$  yields a finite diagrammatic certificate.

This leads to ropelength-filtered Reidemeister graphs

$$G_{\Lambda,u}^{\text{Reid}}(K),$$

whose vertices are diagrams arising from representatives in  $Y_\Lambda(K)$  and whose edges are Reidemeister moves appearing under generic deformations. The exact construction may vary depending on the chosen equivalence relation on diagrams, but the role of the graph is fixed: it records finite recognition data below the scale  $\Lambda$ .

## 5.3 Discrete knot theory

Discrete knot theory replaces the continuous space itself by a finite move graph. The model is not merely a certificate extracted from a path; it is a finite state space whose connected components are directly computable.

Thus the conceptual distinction is:

$$\text{finite knot theory} = \text{finite recognition data},$$

whereas

$$\text{discrete knot theory} = \text{finite state-space model}.$$

## 5.4 Correspondence diagram

The relations can be summarized schematically by the diagram

$$\begin{array}{ccc} Y_\Lambda(K) & \xrightarrow{\text{generic projection}} & G_{\Lambda,u}^{\text{Reid}}(K) \\ \downarrow \text{lattice discretization} & & \uparrow \text{finite certificate} \\ G_N^{\mathcal{L},\mathcal{M}}(K) & \xrightarrow{\text{projection}} & G_{M(N),u}^{\text{fin}}(K). \end{array}$$

Here  $G_{M(N),u}^{\text{fin}}(K)$  denotes a finite diagrammatic graph with complexity bounded by a function  $M(N)$ .

The diagram is not intended as a commutative diagram in a category of graphs. In particular, the lower horizontal arrow is not asserted to be a graph homomorphism on all vertices and edges. It means that a realized lattice path, when projected generically, produces finite diagrammatic data and hence a finite certificate. The arrows have different meanings:

- (i)  $Y_{\Lambda}(K) \rightarrow G_{\Lambda,u}^{\text{Reid}}(K)$  is a projection to finite diagrammatic data.
- (ii)  $Y_{\Lambda}(K) \rightarrow G_N^{\mathcal{L},\mathcal{M}}(K)$  is a discretization or surrogate construction.
- (iii)  $G_N^{\mathcal{L},\mathcal{M}}(K) \rightarrow G_{M(N),u}^{\text{fin}}(K)$  sends lattice paths to finite Reidemeister certificates.
- (iv) The reverse direction from finite data to lattice data is a realization problem.

## 6 Discrete paths as finite certificates

A key advantage of the lattice model is that an explicitly realized discrete path can be converted into finite diagrammatic data. The following formulation makes the required hypothesis on the local move system explicit.

**Definition 6.1** (PL-realizable local move system). A local move system  $\mathcal{M}_{\mathcal{L}}$  is called *PL-realizable* if every allowed local move  $\omega \rightsquigarrow \omega'$  admits an ambient PL isotopy  $H_t$  of  $\mathbb{R}^3$ , supported in a ball meeting the polygon only in the local move region, such that  $H_0(\omega) = \omega$ ,  $H_1(\omega) = \omega'$ , and  $H_t(\omega)$  is an embedded polygonal knot for all  $t$ . This is an additional hypothesis on the move system, not a formal consequence of self-avoidance of the endpoints.

**Remark 6.2** (Cubulated moves). The cubulated move system of Hinojosa–Verjovsky–Verjovsky Marcotte [6] provides a natural example of a PL-realizable local move system in the sense of the preceding definition. It is known that cubulated moves generate ambient isotopy for cubic knots, and each individual cubulated move is supported in a ball and can be realized by a PL ambient isotopy. In contrast, we do not claim here that BFACF moves form a complete move system, and we do not need BFACF completeness for the seed-generated computations below.

**Theorem 6.3** (Discrete-to-finite projection). *Let  $\mathcal{M}_{\mathcal{L}}$  be PL-realizable, and let  $\omega_0, \omega_1, \dots, \omega_r$  be a path in  $G_N^{\mathcal{L},\mathcal{M}}(K)$ . For a generic projection direction  $u$ , the projected diagrams*

$$D_u(\omega_0), D_u(\omega_1), \dots, D_u(\omega_r)$$

*are related by a finite sequence of Reidemeister moves after subdividing each local move into a generic one-parameter PL isotopy. Consequently, every realized discrete admissible path gives a finite Reidemeister certificate.*

*Proof.* For each edge  $\omega_i \rightsquigarrow \omega_{i+1}$  choose the PL ambient isotopy provided by the PL-realizability hypothesis. Concatenating these finitely many isotopies gives a PL one-parameter family from  $\omega_0$  to  $\omega_r$ . After subdividing the time interval, this family is linear on finitely many parameter subintervals and has only finitely many vertices and edges at each time.

Choose a projection direction outside the finite union of exceptional directions where an edge is projected to a point or where two non-adjacent edges have a non-isolated projected overlap. A further arbitrarily small generic perturbation of the PL isotopy, fixed at the endpoints of the move intervals, makes the projected one-parameter family generic in the usual Reidemeister sense: away from finitely many times the diagram is regular, and at each singular time exactly one standard local event occurs. By the PL version of Reidemeister’s theorem [13, 2], the change in the diagram over each move interval is therefore a finite sequence of Reidemeister moves. Since the lattice path has finitely many edges, the concatenated projected change is finite.  $\square$

**Corollary 6.4** (Discrete merge certificates). *Suppose two initial lattice components  $C, D$  merge at level  $N$ , that is,*

$$m_{\mathcal{L}, \mathcal{M}}(C, D) = N,$$

*and suppose the chosen local move system is PL-realizable. Then, for a generic projection direction  $u$ , any chosen lattice path realizing the merge projects to a finite Reidemeister certificate.*

*Proof.* A merge at level  $N$  is represented by a finite path in  $G_N^{\mathcal{L}, \mathcal{M}}(K)$  connecting a representative of  $C$  to a representative of  $D$ . Apply Theorem 6.3 to this path.  $\square$

**Remark 6.5.** One may seek uniform bounds of the form

$$M(N) \leq CN^2$$

for diagrammatic crossing complexity, since a polygon with  $N$  edges has at most quadratically many pairs of edges. For move paths, however, the number of Reidemeister moves also depends on the length of the chosen path and on the projection direction. Thus the most robust statement is the existence of a finite certificate for a realized path, not a sharp universal complexity bound.

## 7 From finite data back to discrete models

The reverse direction is possible but should be formulated as a realization principle rather than as an equivalence of theories.

**Definition 7.1** (Finite-to-discrete realization property). A finite diagrammatic model is said to have the *finite-to-discrete realization property* with respect to a lattice model  $\mathfrak{D} = (\mathcal{P}^{\mathcal{L}}(K), \mathcal{M}_{\mathcal{L}}, \ell)$  if the following hold.

- (i) Every diagram in the finite model can be realized by a lattice polygon.
- (ii) Every Reidemeister move in the finite model can be realized by a finite sequence of lattice local moves in the chosen move system.
- (iii) There is a complexity-control function  $Q$  such that diagrams of finite complexity at most  $M$  are realized by lattice polygons of length at most  $Q(M)$ .

**Proposition 7.2** (Conditional finite-to-discrete lifting). *Assume the finite-to-discrete realization property. Then any finite Reidemeister path of diagrammatic complexity at most  $M$  lifts, relative to the chosen realization scheme, to a path in  $G_{Q'(M)}^{\mathcal{L}, \mathcal{M}}(K)$  for some complexity-control function  $Q'$ .*

*Proof.* Realize each diagram in the path by a lattice polygon using condition (i). Realize each Reidemeister move by a finite sequence of lattice local moves using condition (ii). Taking the maximum lattice length over the finitely many intermediate lattice polygons gives a bound. The assumed complexity control provides a function  $Q'$  depending only on the chosen finite complexity bound and the realization scheme.  $\square$

**Remark 7.3.** This statement is deliberately conditional. It avoids asserting that finite knot theory and discrete knot theory are equivalent. In particular, condition (ii) is a substantive assumption for any specific local move system. We do not claim here that arbitrary Reidemeister moves lift to BFACF paths with controlled length. The correct interpretation is that finite diagrammatic data can often be implemented in sufficiently fine or sufficiently large lattice models, but the construction requires explicit realization and complexity control.

## 8 Relation to ropelength-filtered spaces

We now indicate how the lattice-filtered model relates to the original ropelength-filtered space.

### 8.1 Lattice polygons as thick representatives

A raw lattice polygon is not a smooth curve and has corners. To compare it with ropelength theory, one may round the corners and thicken the polygon. To avoid collisions under smoothing, it is useful to impose a discrete thickness condition.

**Definition 8.1** (Combinatorially thick lattice polygon). Let  $\rho > 0$ . A lattice polygon  $\omega$  is called  $\rho$ -thick if there are pairwise disjoint closed regular neighborhoods of radius  $\rho$  for all non-adjacent edges and pairwise disjoint corner balls in which the incident edge neighborhoods meet only in the prescribed adjacent way. This condition is part of the hypothesis; it is not automatic for arbitrary lattice polygons.

**Proposition 8.2** (Smoothing estimate). *Fix  $\rho > 0$  and a smoothing convention inside each allowed corner ball. There is a constant  $A_\rho > 0$  such that every  $\rho$ -thick lattice polygon  $\omega$  of lattice length  $N$  admits a smooth representative  $\gamma_\omega$  of the same knot type with*

$$\text{Thi}(\gamma_\omega) = 1, \quad \text{Len}(\gamma_\omega) \leq A_\rho N.$$

*Proof.* Inside each corner ball replace the two incident straight subarcs by the fixed rounded arc prescribed by the smoothing convention, and shorten the adjacent straight portions accordingly. The  $\rho$ -thick hypothesis gives disjoint control neighborhoods for non-adjacent edges and for the corner balls, so these local replacements cannot create a new intersection between non-adjacent parts of the curve. Hence the rounded curve is ambient isotopic to the original lattice polygon. The same neighborhood control gives a positive lower bound, depending only on  $\rho$  and the smoothing convention, for the reach of the rounded curve. After scaling so that the thickness is 1, the length is multiplied by a constant depending only on that lower bound. Since the original polygon has  $N$  unit edges and the smoothing changes length by a bounded amount per corner, the final length is at most  $A_\rho N$ .  $\square$

Thus there is a coarse comparison map on the  $\rho$ -thick subfamily,

$$\mathcal{P}_N^{\mathcal{L},\rho}(K) \longrightarrow Y_{A_\rho N}(K),$$

where  $\mathcal{P}_N^{\mathcal{L},\rho}(K)$  denotes the set of  $\rho$ -thick lattice polygons of length at most  $N$ . No such map is asserted for arbitrary non-thick lattice polygons.

### 8.2 What should not be claimed

The preceding comparison does not imply that

$$G_N^{\mathcal{L},\mathcal{M}}(K)$$

is equivalent to

$$Y_\Lambda(K).$$

There are several reasons:

- (i) lattice polygons form only a discrete subset of all thick representatives;
- (ii) local lattice moves do not encode all continuous deformations at a fixed scale;
- (iii) the relation between lattice length and ropelength is coarse and depends on the smoothing convention;

(iv) merge scales in the lattice model may depend on the lattice and move system.

Therefore the lattice model is best regarded as a computable surrogate rather than a canonical discretization.

### 8.3 A convergence problem

One may nevertheless ask whether finer and finer lattice models approximate the continuous theory.

**Problem 8.3** (Convergence of discrete merge scales). *Let  $a > 0$  be a mesh size and consider lattice polygons in  $a\mathbb{Z}^3$  with a suitable discrete thickness condition. Define lattice merge scales after normalizing length by  $a$ . Under what conditions do the resulting discrete merge scales converge, or at least give upper and lower bounds, for the continuous ropelength merge scales as  $a \rightarrow 0$ ?*

This problem is central if one wants to promote discrete knot theory from a computable surrogate to an approximation theory for ropelength-filtered knot spaces. The difficulty is twofold. First, the vertex sets must approximate thick smooth knots while retaining a uniform discrete thickness condition. Second, the move system must approximate controlled ambient isotopies without introducing artificial barriers or shortcuts. Possible approaches include using thickness-preserving cubical moves, proving rounding-and-straightening estimates with explicit reach control, or comparing upper and lower merge barriers through coarse Lipschitz maps between the lattice and ropelength filtrations.

## 9 Computability

At each fixed level, the discrete theory is finite.

**Theorem 9.1** (Finite computability). *Let  $\mathfrak{D}(K) = (\mathcal{S}(K), \mathcal{M}, \ell)$  be a filtered local-move model. For each  $N$ , the following data are computable by finite graph procedures, provided the finite set  $\mathcal{S}_N(K)$  and the move relation are effectively enumerated:*

- (i) the graph  $G_N^{\mathfrak{D}}(K)$ ;
- (ii) its connected components  $\pi_0(G_N^{\mathfrak{D}}(K))$ ;
- (iii) the image of each component under the inclusion to higher levels;
- (iv) the merge scale of any two initial components, up to any prescribed search bound.

*Proof.* The graph is finite by assumption. Connected components are computable by standard breadth-first or depth-first search. The inclusion maps are obtained by identifying the same vertices in the nested graphs. To compute merge scales up to a search bound  $B$ , compute the components of  $G_N^{\mathfrak{D}}(K)$  for  $N_0 \leq N \leq B$  and record the first level at which the two initial components have the same image.  $\square$

**Remark 9.2.** The theorem is an effective finiteness statement rather than an efficient algorithmic complexity theorem. Enumeration of lattice knots of length at most  $N$  is itself difficult for large  $N$ . Nonetheless, the problem is finite and well-defined, in contrast with the direct computation of path components of  $Y_\Lambda(K)$ .

## 10 A prototype implementation

The preceding computability statement is abstract. For the purposes of experimentation, we implemented a small Python prototype for the simple cubic lattice. The program is not intended as an optimized enumeration engine; rather, it is a transparent implementation of the definitions above. Its role is to construct the BFACF-filtered graph from a supplied finite list of lattice polygons, or to explore the reachable subgraph from specified seed polygons.

The prototype represents a lattice polygon as a cyclic list of vertices in  $\mathbb{Z}^3$ . It canonicalizes polygons up to translation, cyclic reparametrization, reversal of orientation, and proper cubic rotations. If one wishes to identify mirror images, the full cubic symmetry group may be used instead. It then generates three BFACF-type moves:

- (i) length-preserving corner flips;
- (ii) positive edge expansions, increasing lattice length by 2;
- (iii) negative edge contractions, decreasing lattice length by 2.

Only moves whose outputs remain self-avoiding lattice polygons are retained. Thus, for a supplied finite vertex set  $V \subset \mathcal{P}_N^{\text{SC}}(K)$ , the program constructs the induced graph

$$G_N^{\text{SC,BFACF}}(K)|_V.$$

It then computes connected components by breadth-first search.

The following command explores the reachable BFACF graph from the square unknot up to length 8:

```
python lattice_bfacf_graph.py --demo-unknot --max-len 8
```

The output of this elementary test is:

```
Demo: square unknot, BFACF reachable graph up to length 8
vertices: 18
edges:    31
components: 1
component sizes: [18]
```

This confirms, at the level of the prototype, that the reachable subgraph from the square unknot remains connected through length 8.

For non-trivial knots, the program expects an external enumeration of lattice polygons. For example, if `trefoil24.json` contains a list of length 24 trefoil polygons, then the induced graph at the minimal level is built by

```
python lattice_bfacf_graph.py --input trefoil24.json --max-len 24
```

If `trefoil_seed.json` contains one or more seed polygons, then the reachable graph below length 26 can be explored by

```
python lattice_bfacf_graph.py --input trefoil_seed.json --max-len 26 --explore
```

Thus the implementation separates two tasks. The enumeration of all polygons of a given knot type and length is supplied externally, while the construction of the filtered BFACF graph, the computation of connected components, and the calculation of merge data are performed by the program. In the version used for the longer braid-generated seed below, canonicalization is implemented through cyclic edge sequences rather than by enumerating all translated cyclic vertex lists; this gives the same canonical quotient in the examples considered here and makes longer seed computations feasible.

**Remark 10.1.** This separation is important for the trefoil. The complete enumeration of all length 24 trefoils in the simple cubic lattice is a substantial lattice-knot enumeration problem. The present code is designed to use such data once supplied; it does not, by itself, enumerate all minimal trefoils from scratch.

For the experiments reported below, we used the input files listed in Table 1.

file	role	knot type or experiment
<code>trefoil_seed.json</code>	seed polygon	$3_1$
<code>figure8_seed.json</code>	seed polygon	$4_1$
<code>figure8_mirror_seed.json</code>	reflected seed polygon	$4_1!$
<code>figure8_and_mirror_seeds.json</code>	two-seed input	$4_1$ and $4_1!$
<code>fiveone_seed.json</code>	seed polygon	$5_1$
<code>fivetwo_braid_seed.json</code>	stress-test seed	non-minimal $5_2$ input
<code>granny_seed.json</code>	sanity-check seed	$3_1\#3_1$
<code>square_seed.json</code>	sanity-check seed	$3_1\#3_1!$
<code>granny_square_seeds.json</code>	two-seed input	composite-trefoil sanity check

Table 1: Input files used in the seed-generated experiments. The  $5_2$  braid seed is a non-minimal stress-test input and is not used as birth-level evidence for  $5_2$ .

Unless explicitly stated otherwise, computations were run without the `--mirror` option, so that mirror symmetries are not identified. This convention is essential when one wants to compare mirror-sensitive examples.

## 11 Reproducible seed-generated experiments

This section reports small reproducible computations with the prototype code. The purpose is not to enumerate complete minimal layers, except where explicitly stated. Instead, the computations test seed-generated BFACF subgraphs and provide finite certificates for separation or merging at specified length levels. A table entry marked “seed-generated” is exhaustive only for the component generated from the supplied seed under the stated length bound. A table entry with a cap is a partial exploration and is not used as evidence for global connectivity.

### 11.1 The unknot

For the unknot, the minimal lattice layer consists of shortest lattice unknots. In the simple cubic lattice these are square polygons of length 4, up to lattice isometry. The prototype computation gives a basic check: the BFACF-reachable subgraph from the square unknot through length 8 has 18 vertices, 31 edges, and one connected component.

### 11.2 The trefoil in the simple cubic lattice

The first non-trivial example is the trefoil  $3_1$ . It is known that every non-trivial polygon in the simple cubic lattice has length at least 24, and that the trefoil is realized at this length [7, 8, 5]. Hence

$$n_{\text{SC}}(3_1) = 24.$$

Known enumeration data for minimal simple cubic trefoils show that, counting both chiralities in the standard population convention, there are 3328 trefoil polygons of length 24, falling into 142 symmetry classes. The next two even levels are already much larger; see Table 2.

The prototype gives the seed-generated checks summarized in Table 3. Starting from the supplied 24-edge trefoil seed, the BFACF-reachable subgraph with  $\ell \leq 24$  has 56 canonical vertices, 127 edges, and one connected component. Raising the bound to 26 and stopping after

$N$	$P_N(3_1)$	$S_N(3_1)$
24	3328	142
26	281208	11721
28	14398776	599949

Table 2: Enumeration data for simple cubic trefoils quoted from the lattice-knot literature. These are not new computations in the present paper.

1000 vertices gives a partial exploration with 2164 edges and one connected component. These numbers do not enumerate the entire minimal layer  $I_{SC}(3_1)$ ; they describe one seed-generated BFACF component.

### 11.3 The figure-eight knot in the simple cubic lattice

For the figure-eight knot  $4_1$ , the minimal simple cubic lattice length is

$$n_{SC}(4_1) = 30.$$

Published enumeration data give

$$P_{30}(4_1) = 3648, \quad S_{30}(4_1) = 152$$

[5, 9]. Using the supplied seed file, the BFACF-reachable subgraph at the birth level has 58 vertices, 118 edges, and one connected component; see Table 3. Allowing length up to 32 and imposing a cap of 1000 vertices gives a partial reachable subgraph with 1000 vertices, 2137 edges, and one connected component.

$K$	$n_{SC}(K)$	level $N$	mode	cap	$ V $	$ E $
$3_1$	24	24	seed-generated	none	56	127
$3_1$	24	26	capped	1000	1000	2164
$4_1$	30	30	seed-generated	none	58	118
$4_1$	30	32	capped	1000	1000	2137
$5_1$	34	34	seed-generated	none	5	4
$5_1$	34	36	capped	1000	1000	2207

Table 3: Seed-generated and capped BFACF computations used in the paper. The capped rows are partial explorations.

The comparison between the  $3_1$  and  $4_1$  birth-level seeds suggests that local BFACF structure and global minimal-layer population are different kinds of data: the known birth layers have very different enumeration sizes, but the chosen seed components are of comparable size.

### 11.4 The figure-eight knot and its mirror

The figure-eight knot is amphichiral: topologically,  $4_1$  is equivalent to its mirror image  $4_1!$ . This makes it a useful test case for separating ordinary topological equivalence from connectivity inside a length-filtered lattice move graph. The distinction is move-system-dependent: the calculation below concerns BFACF paths, not arbitrary lattice isotopies.

Starting from the 30-edge simple cubic lattice representative used above, we formed a reflected mirror seed by applying the lattice reflection

$$(x, y, z) \mapsto (-x, y, z).$$

We then explored the BFACF-reachable graph generated by the two seeds under the minimal length bound  $\ell \leq 30$ . When mirror symmetries are not identified, the computation gives 116 vertices, 236 edges, and two components of sizes 58 and 58. If mirror symmetries are identified during canonicalization, the same input gives 58 vertices, 118 edges, and one component. These two checks are summarized in Table 4.

input	mirror identified?	$N$	$ V $	$ E $	$\#\pi_0$
$(4_1, 4_1!)$	no	30	116	236	2
$(4_1, 4_1!)$	yes	30	58	118	1

Table 4: Mirror comparison for the supplied figure-eight seed and its reflected mirror seed.

**A seed-generated merge-scale check and certificate.** The preceding computation shows that the two seed-generated BFACF components do not merge at level  $N = 30$ . Since BFACF moves change lattice length by  $0, \pm 2$ , the next possible BFACF length level is  $N = 32$ . The supplementary script `merge_check_bfacf.py` performs a bidirectional search between two supplied seeds. For the figure-eight seed and its reflected mirror seed, the level 30 check returns `connected=false` with status `frontier_exhausted`. This status means that the two seed-generated frontiers are exhausted under the length bound  $N \leq 30$ , not that a state or time cap was reached. With mirror symmetries identified, the level 30 check returns `connected=true` with status `same_canonical_state`.

At the candidate merge level  $N = 32$ , the command recorded in the supplementary README returned

```
connected=true,      status=connecting_state_found.
```

The JSON summary records 3036 discovered states from the first search frontier, 10741 discovered states from the second frontier, and 11761 expanded states. The first two numbers count discovered states in the two frontiers at the stopping time, whereas the last number counts states actually removed from a queue and expanded; they are therefore not expected to add up. The recorded runtime for this run was 851.825 seconds. Runtime is hardware-dependent; the supplementary README records the Python/Linux configuration used for the archived run.

In addition to the connectivity summary, we extracted an explicit BFACF path realizing the merge at level  $N = 32$ . The path consists of 21 states and 20 BFACF moves. It passes through a 32-edge connecting state  $\eta$ : the original 30-edge seed  $\omega$  reaches  $\eta$  in 5 BFACF moves, while the reflected mirror seed  $\omega!$  reaches the same state  $\eta$  in 15 BFACF moves. The edge-number sequence along the extracted full path is

30, 32, 32, 32, 32, 32, 32, 32, 32, 32, 30, 32, 32, 32, 32, 32, 32, 30, 30, 30, 30.

Thus the maximum length along the path is 32, giving an explicit certificate for the seed-generated merge at  $N = 32$ ; see Figure 1.

Since the two seed-generated BFACF components are separated at  $N = 30$ , and since there is no intermediate BFACF length level, we obtain the exact seed-generated BFACF merge scale

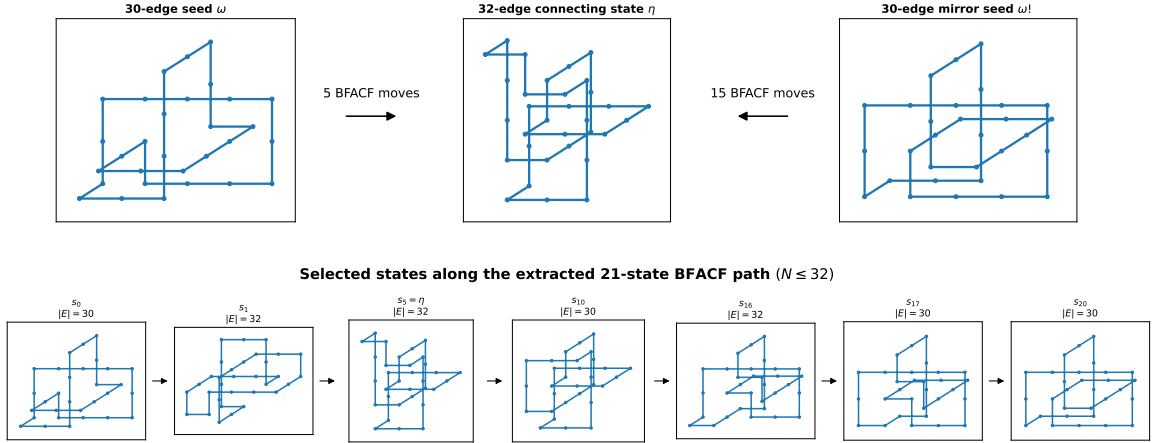
$$m_{\text{seed}}^{\text{BFACF}}(\omega, \omega!) = 32.$$

**Observation 11.1** (A length-two BFACF mirror barrier for the figure-eight seed). *For the supplied 30-edge simple cubic figure-eight seed  $\omega$  and its reflected mirror seed  $\omega!$ , with mirror symmetries not identified, the seed-generated BFACF merge scale is*

$$m_{\text{seed}}^{\text{BFACF}}(\omega, \omega!) = 32.$$

*Equivalently, the two seeds are separated at the minimal level  $N = 30$  and become connected after allowing two additional lattice edges.*

### A seed-generated BFACF path for the figure-eight knot at $N = 32$



Extracted full path: 21 states, 20 BFACF moves. The two seed-generated components are disconnected at  $N = 30$  and connected at  $N = 32$ .

$$m_{\text{seed}}^{\text{BFACF}}(\omega, \omega!) = 32$$

Figure 1: An extracted BFACF path connecting the supplied 30-edge figure-eight seed  $\omega$  to its reflected mirror seed  $\omega!$  under the length bound  $N = 32$ . The two search branches meet at a 32-edge state  $\eta$ . The seed  $\omega$  reaches  $\eta$  in 5 BFACF moves, while the mirror seed  $\omega!$  reaches  $\eta$  in 15 BFACF moves. Hence the full extracted path has 21 states and 20 moves, and gives an explicit certificate for  $m_{\text{seed}}^{\text{BFACF}}(\omega, \omega!) = 32$ .

The statement is seed-generated and BFACF-specific. It is not a global merge scale for the entire minimal layer  $I_{\text{SC}}(4_1)$ . Other symmetry classes among the 152 minimal classes of  $4_1$  could have different BFACF merge behavior, and a larger complete move system could merge the same two seeds no later than BFACF.

### 11.5 The five-crossing knots

The two prime knots with five crossings have the same crossing number but occupy different levels in the simple cubic lattice filtration. Published enumeration data give

$$n_{\text{SC}}(5_1) = 34, \quad n_{\text{SC}}(5_2) = 36,$$

and minimal populations

$$P_{34}(5_1) = 6672, \quad P_{36}(5_2) = 114912$$

[5]. Thus the birth level already distinguishes the two five-crossing prime knots in the simple cubic lattice filtration.

For  $5_1$  we used a 34-edge minimal simple cubic lattice representative. The birth-level seed-generated graph is very small: it has 5 vertices, 4 edges, and one component. This indicates that the supplied minimal  $5_1$  seed is locally quite rigid at the birth level: only a few length-preserving BFACF corner changes are available before one leaves the length-34 layer. Allowing length up to 36 and stopping after 1000 vertices gives a partial exploration with 2207 edges and one component; see Table 3.

For  $5_2$ , the supplied test seed is not a minimal 36-edge representative. Instead, it is a cubical closed-braid seed of length 238. We now treat this calculation only as an implementation stress test, not as evidence about the birth layer of  $5_2$ . With length bound 238 and cap 1000, the

explored subgraph has 1000 vertices, 1043 edges, and one component. A genuine birth-level experiment for  $5_2$  would require a curated list of minimal 36-edge representatives and should replace this stress test in a future version.

## 11.6 Composite trefoil examples as a sanity check

We also made a very small sanity check using two non-minimal composite trefoil seeds: the granny knot  $3_1\#3_1$  and the square knot  $3_1\#3_1!$ . These knots are topologically distinct, for example by chirality-sensitive polynomial invariants [10]. The purpose of the present computation is not to prove or rediscover this distinction. It only checks that the implementation keeps two known different seed types separated in a tiny capped exploration.

The seeds have length 66. Running the two seeds separately with a cap of 20 vertices gives one component in each explored subgraph. Running the two seeds together, without mirror identification and with a cap of 40 vertices, gives 40 vertices, 40 edges, and two components of sizes 29 and 11. Because the cap is extremely small relative to the size expected at this length, this check is not used as scientific evidence for a merge-scale claim. It is included only as a reproducibility and consistency test.

## 11.7 Computational interpretation

For a chosen move system, the merge scale

$$m_{\mathcal{L},\mathcal{M}}(C, D)$$

measures the minimal amount of additional lattice length required to pass from one component to another using moves in  $\mathcal{M}$ . It is therefore a discrete, move-system-dependent energy-barrier invariant. The shifted value

$$m_{\mathcal{L},\mathcal{M}}(C, D) - n_{\mathcal{L}}(K)$$

measures the extra length required beyond the minimal lattice length. The experiments above should be read in exactly this relative sense: they are reproducible computations in explicitly specified finite BFACF graphs.

## 12 Further questions

The framework suggests several natural problems.

The computations also suggest the following experimental conjectures.

**Conjecture 12.1** (Positive lattice amphichirality barrier). *There exist amphichiral knot types  $K$  and minimal simple cubic lattice representatives  $\omega$  such that  $\omega$  and its reflected mirror seed are not connected in the minimal BFACF graph, but merge at a strictly higher level. The figure-eight computation above gives seed-generated evidence with barrier  $32 - 30 = 2$ .*

**Conjecture 12.2** (Birth level is only a first-order invariant). *For small prime knots, the simple cubic birth level  $n_{\text{SC}}(K)$  gives a useful coarse filtration, but the component structure of  $G_{n_{\text{SC}}(K)}^{\text{SC,BFACF}}(K)$  and the corresponding merge scales contain strictly finer information.*

**Problem 12.3** (Dependence on move system). *Compare the merge ultrapseudometrics obtained from BFACF-type moves and from cubulated moves. When do they define the same hierarchical clustering of the minimal lattice layer?*

**Problem 12.4** (Dependence on lattice). *Compare the discrete merge scales obtained from the simple cubic, body-centered cubic, and face-centered cubic lattices. Which features are lattice-independent?*

**Problem 12.5** (Stable discrete merge scale). *Does some stabilization procedure, such as lattice refinement or controlled subdivision, produce a merge invariant of  $K$  that is independent of the chosen lattice?*

**Problem 12.6** (Comparison with ropelength). *Find explicit functions  $A, B$  such that lattice merge scales give upper or lower bounds for ropelength merge scales:*

$$A m_{\mathcal{L}, \mathcal{M}}(C, D) \leq m_{\text{rop}}(C', D') \leq B m_{\mathcal{L}, \mathcal{M}}(C, D),$$

where  $C', D'$  are suitable continuous counterparts of  $C, D$ .

**Problem 12.7** (Finite recognition length from lattice graphs). *Use lattice-filtered move graphs to define a finite recognition length  $L_{\text{char}}^{\mathcal{L}}(K)$ : the first lattice length level at which a finite diagrammatic pattern recognizing  $K$  appears in the projection of the lattice graph.*

## Code and data availability

A prototype Python implementation accompanies this paper. The script constructs BFACF-filtered move graphs from supplied finite lists of simple cubic lattice polygons, computes connected components, and records summary data. The supplementary archive contains the main script `lattice.bfacf_graph.py`, the merge-check script `merge_check_bfacf.py`, the braid-seed helper `make_braid_seed.py`, a README file with the reproduction commands, and the JSON seed and summary files used in the experiments.

The supplied data include the trefoil seed; the figure-eight seed, its reflected mirror seed, and the combined mirror-comparison input; the  $5_1$  seed and the non-minimal braid-generated  $5_2$  stress-test seed; and the granny/square knot sanity-check seeds. The JSON summary files record the computations reported in the text, including the  $4_1$ -mirror merge check at  $N = 32$ , the  $5_1$  runs at  $N = 34$  and  $N = 36$ , and the braid-generated  $5_2$  stress test at  $N = 238$ . The archive also includes the extracted explicit  $N = 32$  merge certificate `figure8_merge_path_32.json`, its summary file, and the certificate figure used in Figure 1.

The implementation is intended as a transparent prototype rather than an optimized enumeration engine. In particular, the enumeration of all lattice representatives of a fixed knot type and length must be supplied externally. The summary files reported here record only the seed-generated or capped searches specified in the text. The merge-check script returns one of three outcomes at a tested level: a connecting state is found, one frontier is exhausted and hence the two seeds are separated at that level, or a state/time cap is reached and the test is inconclusive.

For the bidirectional merge script, the fields `states_from_seed_1` and `states_from_seed_2` count discovered states in the two search frontiers at the stopping time. The field `expanded` counts states actually expanded from the queues. Thus these quantities measure different aspects of the search and should not be added. The runtime field is hardware-dependent; the archived README records the Python and machine information used for the supplied summaries. The supplementary code and data used for the computations in this paper are archived on Zenodo at DOI: [10.5281/zenodo.20412976](https://doi.org/10.5281/zenodo.20412976). The same material is also included in the arXiv ancillary files accompanying this preprint.

## Declaration of generative AI and AI-assisted technologies

During the preparation of this manuscript, the author used ChatGPT (OpenAI, GPT-5.5 Thinking) for language polishing, organizational suggestions, preliminary consistency checks, and assistance in drafting some explanatory text and code comments. The mathematical definitions, statements, proofs, computations, references, code, and conclusions were checked and verified by the author, who takes full responsibility for the content of the paper.

## 13 Conclusion

We have introduced lattice-filtered move graphs as a finite-state experimental model for knot types. The construction is motivated by ropelength-filtered knot spaces, but it is deliberately computable: representatives are finite lattice polygons, deformations are finite sequences of local moves, and component persistence is measured in finite graphs. The resulting merge scales give a hierarchical, ultrapseudometric structure on initial components whenever the relevant components eventually merge.

The main experimental conclusion is that the chosen BFACF model detects finite move-system-dependent length barriers not visible from ordinary knot type alone. For the figure-eight knot, a minimal seed and its reflected mirror seed are topologically equivalent, but in the seed-generated BFACF graph they are separated at the minimal lattice level and merge at  $N = 32$ . Thus seed-generated BFACF graphs provide a concrete setting in which amphichirality and chirality-sensitive phenomena can be tested by reproducible finite searches, while keeping clear the distinction between seed-specific BFACF computations and global statements about all minimal representatives. The next step is to replace the remaining non-minimal or capped experiments by complete birth-level computations for curated lists of minimal representatives, especially for the five-crossing knots.

## References

- [1] J. W. Alexander and G. B. Briggs, On types of knotted curves, *Ann. of Math.* **28** (1926/27), 562–586.
- [2] G. Burde, H. Zieschang and M. Heusener, *Knots*, 3rd revised and extended ed., De Gruyter Studies in Mathematics, vol. 5, De Gruyter, 2014.
- [3] E. J. Janse van Rensburg and S. G. Whittington, The BFACF algorithm and knotted polygons, *J. Phys. A: Math. Gen.* **24** (1991), 5553–5567.
- [4] E. J. Janse van Rensburg and S. D. Promislow, Minimal knots in the cubic lattice, *J. Knot Theory Ramifications* **4** (1995), 115–130.
- [5] E. J. Janse van Rensburg and A. Rechnitzer, Minimal knotted polygons in cubic lattices, *J. Stat. Mech. Theory Exp.* (2011), P09008.
- [6] G. Hinojosa, A. Verjovsky and C. Verjovsky Marcotte, Cubulated moves and discrete knots, *J. Knot Theory Ramifications* **22** (2013), 1350079.
- [7] Y. Diao, Minimal knotted polygons on the cubic lattice, *J. Knot Theory Ramifications* **2** (1993), 413–425.
- [8] Y. Diao, The number of smallest knots on the cubic lattice, *J. Stat. Phys.* **74** (1994), 1247–1254.
- [9] K. Hong, S. No and S. Oh, Upper bounds on the minimum length of cubic lattice knots, *J. Phys. A: Math. Theor.* **46** (2013), 125001.
- [10] V. F. R. Jones, A polynomial invariant for knots via von Neumann algebras, *Bull. Amer. Math. Soc.* **12** (1985), 103–111.
- [11] R. A. Litherland, J. Simon, O. Durumeric and E. Rawdon, Thickness of knots, *Topology Appl.* **91** (1999), 233–244.
- [12] M. Ozawa, *The Ideal Stratum and Deformation Persistence of Knot Types*, arXiv:2604.17905, 2026.

[13] K. Reidemeister, *Knotentheorie*, Springer, Berlin, 1932.